Free fall motion of a floating body: bubble formation and its effect

Shi Yan Sun, Guo Xiong Wu*, Gang Xu

School of Naval Architecture and Ocean Engineering, Jiangsu University of Science and Technology, Zhenjiang, 212003, China

Abstract: The hydrodynamic problem of a floating body moving downwards into water with prescribed velocity or in free fall motion is solved based on the incompressible velocity potential theory through the boundary element method in the time domain. In particular, the focus is on the whole process of flow detachment, the formation of an open cavity, closure of the cavity or formation of entrapped air bubble, collision of the inner jet with the body surface and jet impact with free surface. The whole problem is divided into several stages and methodology is introduced to resolve the numerical challenge at each stage. In particular the dual coordinate system method is adopted to resolve the local sharp spatial and temporal variation in the impact zone, and the domain decomposition method with Riemann second sheet is adopted to resolve domain overlapping. An auxiliary function method is used to decouple the nonlinear mutual dependence of fluid loading, body motion and bubble deformation. Simulations are undertaken for a floating body moving into water at constant velocity or constant acceleration, and in free motion, respectively. Detailed results for pressure, free surface profile, bubble deformation and body motion are provided, and their physical implications are discussed.

Keywords: Floating body sinking into water; open cavity and closed bubble; fluid/fluid and fluid/structure impact; domain decomposition method; boundary element method.

1. Introduction

The study on the air bubble formed during water entry or a floating body moving into water has a long history. Gilbarg and Anderson [1] undertook experimental study on the bubble formed during a solid body striking a liquid surface. The major factors, the velocity of the body and the atmospheric density or pressure, which affected cavity formation and development, were investigated. Richardson [2] did a similar experiment through shooting a solid sphere into a liquid inside a tank, and the acoustic wave generated during water entry was studied. It was found that the major contribution to the sound came from the pulsations of the air bubble formed behind the body. Duez et al. [3] took the visual and audio recordings for two spheres entering water separately, which had different wettability through a nanometric coating on their surfaces. The results revealed that the condition for an air bubble to be formed was that the impact velocity should be above a critical value which was dependent on the wettability of the sphere.

Much of earlier work on water entry is for an infinite wedge [4-6]. When the gravity is ignored, the flow is self-similar and will be also attached on the body surface. The first requirement for an air bubble to be formed behind a body during water entry is that the liquid has to detach from the body. A typical example is well illustrated in the work of Bao et al. [7, 8]. They considered the problem of a finite wedge entering into water vertically or obliquely. The flow first moved along the wedge surface in the form of a jet, then detached from the knuckle, and an open cavity would be formed as a result. The boundary element method with fully nonlinear dynamic and kinetic boundary conditions was used for the free surface flow, and a continuity condition at the knuckle was incorporated into boundary integral equations to guarantee that the liquid could leave the body

* Corresponding author. Permanent address: Department of Mechanical Engineering, University College London, Torrington Place, London WCIE 7JE, UK. Tel.: +44 20 7679 3870; fax: +44 20 7388 0180.

E-mail address: g.wu@ucl.ac.uk (G.X. Wu)

surface smoothly. Other important work on open cavity with boundary element method includes Zhao et al. [9] and Wang and Faltinsen [10]. The latter also considered the contraction or collapse of open cavity. However the simulation was terminated before the closure of air bubble. In the above work the body was initially above the water surface and then entered water. Korobkin and Wu [11] considered the case of a semi-circular cylinder which already floated on water surface and then subsequently moved downwards. The problem was solved in the Lagrangian framework and flow detachment was modelled. The functions were expanded in terms of time and the solution was valid for the initial stage. In addition to the velocity potential theory, there have been also studies using Reynolds averaged Navier-Stokes equations and the volume of fluid method (VOF) for the free surface tracking. The typical work includes those by Do-Quang and Amberg [12] for a falling sphere to investigate the effect of wettability and by Iranmanesh and Passandideh-Fard [13] for a truncated horizontal circular cylinder where the flow along the longitudinal direction was studied.

The above work is mainly about an open cavity. In practice, an open cavity will always close as time progresses, when the gravity effect becomes more and more important. One of the earliest experimental studies was undertaken by Gilbarg and Anderson [1]. The open cavity behind the body contracted and closed at some point. At the closure of the open cavity, jets would form due to the collision between cavity surfaces. The volume oscillations of a closed bubble and ripples on the bubble surface during the water entry of a projectile were observed in the experimental work by Grumstrup et al. [14]. It was found that the dominant frequency of oscillation was close to the Minnaert frequency [15] based on the diameter. Moreover, the product of wavelength for the ripple and the frequency of oscillation was approximately equal to the projectile speed. The latter was explained through an analytical solution for a long bubble moving in the irrotational flow of a compressible liquid. Aristoff and Bush [16] undertook both theoretical and experimental investigation for the water entry of a small hydrophobic sphere. They found that at a small bond number where the surface tension was important, the depth at which cavity closure occurred would become increasingly large when the falling speed of body increased, and shallow closure would gradually become deep closure. The above studies have significantly advanced our understanding regarding the characteristics of cavity on water entry. However, while they may be good for some global results, it is still a challenge to have detailed results with high accuracy and resolution.

For a finite body entering water, it is expected that fluid can depart from the body surface, as shown in the experiment for a curved body [3], or a truncated wedge [17]. The departed flow may move towards the centre, cause liquid/liquid collision and a closed cavity can be found [12, 14]. This collision is similar to breaking wave hitting on a wall [18], and two jets would be formed. One of these jets would move inside the cavity towards truncated body surface and further collision is expected. This is very similar to the collapse of a symmetric bubble [1], in which the symmetry line can be treated as a wall. At the final stage, the cavity may depart from the body surface, which is common in some deep closure problems [19]. The present work aims to investigate the entire process of water entry of a body in free fall, including cavity initiation, development and collapse (the inward motion of cavity surface), closure or bubble formation, bubble motion and deformation and its effects. We shall adopt the incompressible velocity potential theory for the fluid flow, while surface tension is ignored. Fully nonlinear boundary conditions are adopted on the deforming free surface and bubble surface, which are tracked by the time stepping method. At each time step, the velocity potential problem is solved by the boundary element method (BEM) which can capture the evolution of the free surface with high resolution. As this is a highly complex process, many

different numerical challenges will arise. A particular difficulty is that the process involves the several collisions occurred at different stages. The first one is when the body starts moving down suddenly and the fluid departs from the body surface, and second one is when cavity surfaces merge, which leads to a liquid to liquid collision. When the bubble is formed, its inner jet will further collide with the body surface. The jet will turn to move along the body surface and then hit the bubble surface again. To account all these collisions, we shall adopt and refine the various methods developed previously. In particular, the numerical condition for flow detachment [7] will be used for initial stage of water entry. The dual system method [20] based on the stretched system method [6] will be used for cavity surface collision and inner jet collision with the body surface. The jet collision with the bubble will be treated using Riemann second sheet [21].

In the following sections, the mathematical model based on incompressible potential flow theory for the body moving downwards into water is first outlined in Sec. 2. Solution procedure is provided in Sec. 3. Specifically, the boundary element method, together with several special schemes for resolving numerical difficulties, are first presented, and the procedure for pressure and the motion of body are then given. Numerical results and discussions are provided in Sec .4, which is followed by Conclusions.

2. Mathematical model

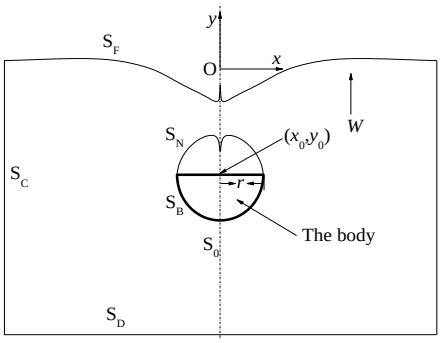

Fig. 1. The sketch of the problem.

The problem which we consider is a body with a horizontal top floating on the calm water surface moving downwards suddenly with an initial velocity W_0. A Cartesian coordinate system $O-xy$ fixed in space is defined, in which x -axis coincides with the horizontal top of the body, and is at the still water level, and y -axis points upwards and passes through the centre of body. The water density ρ, the acceleration due to gravity g and the typical length dimension r of the body, are used for non-dimensionalization. For the body of symmetry, y axis passes through its symmetry line. The inner free surfaces formed after the departure of the fluid from both sides of the body may move inwardly and meet at the later stage on the y axis. Consequently, an air bubble will be formed between the inner free surface S_N and the top of the body surface. The body surface, outer free surface, far field boundary and fluid bottom are respectively denoted as S_B, S_F, S_C and S_D, as shown in Figure 1. (x_0, y_0) is the centre of the horizontal top of the body, which is $(0,0)$ at $t=0$, and whose movement is used to measure the displacement of the falling

body. After the formation of the bubble, an inner jet can be developed along the symmetry line. It will move towards the body and may hit the body at the later stage. After that it will then make a turn and move along the horizontal top of the body, and eventually hit the inner free surface on the other side.

The fluid is assumed to be inviscid and incompressible, and the flow to be irrotational. The potential ϕ can then be introduced. Within the fluid domain, it satisfies the Laplace equation.

$$\nabla^2\phi=0 \tag{1}$$

As we focus on the symmetric problems, only half of the domain with $x \geq 0$ is considered and the symmetry boundary is denoted by S_0. Neglecting the surface tension, the dynamic boundary condition on the outer free surface S_F with the constant atmospheric pressure P_0 can be written as

$$\frac{D\phi}{Dt} = \frac{1}{2}\nabla\phi\cdot\nabla\phi - y \tag{2}$$

in the Lagrangian form. Based on the assumption that the entrapped bubble undergoes an adiabatic process, the pressure inside the bubble can be expressed as

$$P = P_0\left(\frac{V_0}{V}\right)^{\gamma} \tag{3}$$

where V_0 is the volume of the air bubble when it is first entrapped, V is its subsequent volume which varies with time, and γ is the heat ratio of air. Substituting Eq. (3) into the Bernoulli's equation, the dynamic boundary condition on inner free surface S_N can be written as

$$\frac{D\phi}{Dt} = \frac{1}{2}\nabla\phi\cdot\nabla\phi - y - P_0\left[\left(\frac{V_0}{V}\right)^{\gamma} - 1\right] \tag{4}$$

The kinematic boundary conditions on both S_F and S_N in the Lagrangian form can be written as

$$\frac{Dx}{Dt} = \frac{\partial\phi}{\partial x}, \quad \frac{Dy}{Dt} = \frac{\partial\phi}{\partial y} \tag{5}$$

The impermeable boundary condition for the body takes the form

$$\frac{\partial\phi}{\partial n} = Wn_y \tag{6}$$

in which W is the nondimensional vertical velocity of the body and $W = W_0$ at $t = 0$, $\mathbf{n}$ is the normal of body surface pointing out of the fluid domain. Due to symmetry, on S_0 we have

$$\frac{\partial\phi}{\partial x} = 0, \quad x = 0 \tag{7}$$

The impermeable boundary condition at the seabed can be written as

$$\frac{\partial\phi}{\partial n} = 0 \tag{8}$$

At the far field, it is assumed that the disturbance to the fluid by the motion of the body has sufficiently decayed, and thus the boundary condition takes the form of

$$\frac{\partial \phi}{\partial n} = 0 \tag{9}$$

As the water surface is assumed to be flat and the fluid is stationary before the motion of the body, the initial condition at time $t = 0$ can be written as

$$\zeta(x > r, t = 0) = 0, \quad \phi(x > r, 0, t = 0) = 0 \tag{10}$$

where ζ is the elevation of free surface. Based on the Laplace equation and the above boundary conditions together with the initial condition, the fluid/structure interaction problem can then be solved through the boundary element method (BEM) combined with a time matching scheme.

3. Solution procedure

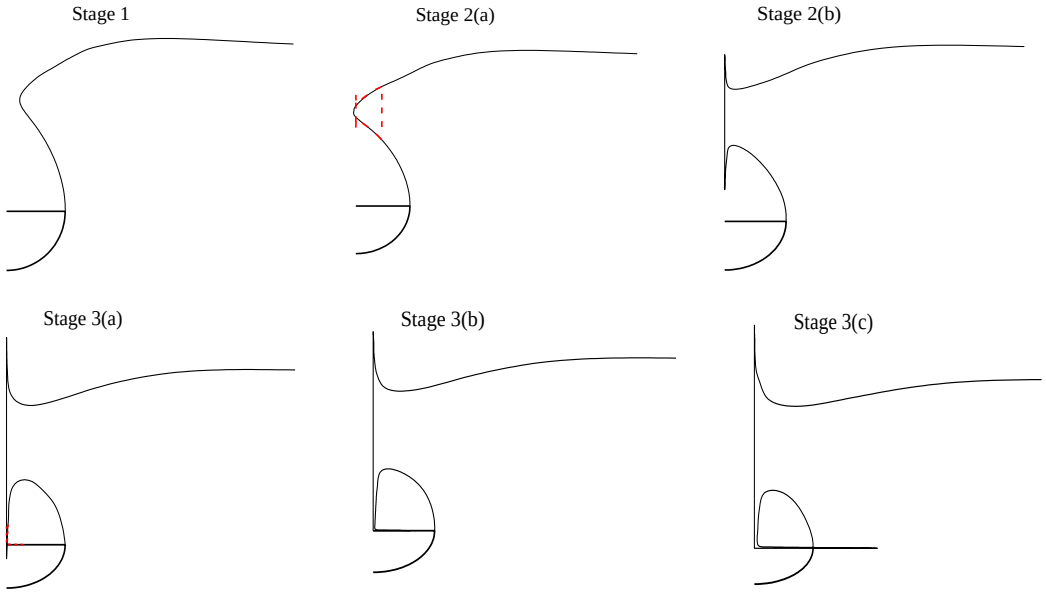

Fig. 2. Different stages of a floating body moving into water. (Stage 1: prior bubble formation, stage 2(a): bubble formation, stage 2(b): development and movement of the inner jet, stage 3(a): collision of the inner jet with the body top, stage 3(b): movement of the horizontal jet, stage 3(c): horizontal jet moving into Riemann second sheet. Solid line: Physical domain; Dash line: Stretched domain)

The whole process of a floating body moving down into water is a complex one. It involves significant amount of domain and boundary changes, jet formation and movement, as well as liquid/liquid and liquid/body collisions. To develop a numerical scheme to meet all these challenges, the overall problem is divided into 3 stages, as shown in Fig. 2. In Stage 1, the water departs from the side of the body and the free surface moves towards the symmetry line, which is similar to an overturning wave moving towards a wall [20]. Stage 2 is between the moment when the inward free surface hits the symmetry line and the inner jet arrives at the top of the body. Stage 2(a) corresponds to the initial period of bubble formation. This is similar to the case of an overturning wave hitting the vertical wall. Two jets will be subsequently developed [20], corresponding to the inner and outer free surfaces respectively. Stage 2(b) is from the moment when the wetted surface on the symmetry line is no longer small, and it covers the period of the inner jet development and movement. Stage 3 is from the moment when the inner vertical jet hits the top of the body. Similar to stage 2, stage 3(a) corresponds to the initial period of vertical jet impact on the body top, and 3(b) is from the moment when the wetted surface on the top of body is no longer small, to the moment when the horizontal jet arrives the inner free surface, and 3(c) starts when the horizontal jet meets the inner

free surface.

3.1. The boundary element method

BEM is used to solve the above boundary value problem for the velocity potential. Through Green's identity, the Laplace equation in the fluid domain can be converted into an integral equation over its whole boundary.

$$A(p)\phi(p) = \int \left[G(p,q)\frac{\partial \phi(q)}{\partial n_{\mathrm{q}}} - \phi(q)\frac{\partial G(p,q)}{\partial n_{\mathrm{q}}} \right] dl_{\mathrm{q}} \tag{11}$$

in which

$$G(p,q) = \ln\sqrt{(x_p - x_q)^2 + (y_p - y_q)^2} \tag{12}$$

and $A(p)$ is the solid angle at point p on the boundary, while the integration is performed with respect to point q. Straight line elements, with variables varying linearly within each element, are distributed along the boundary. The integrations within each element can be obtained explicitly as in Lu et al. [22], and Eq. (11) can be written in matrix form

$$[H]_{N_{\mathrm{d}}\times N_{\mathrm{d}}}[\phi]_{N_{\mathrm{d}}} = [G]_{N_{\mathrm{d}}\times N_{\mathrm{d}}}\left[\frac{\partial \phi}{\partial n}\right]_{N_{\mathrm{d}}} \tag{13}$$

where N_{d} is the total number of nodes over the whole boundary, and the matrices of $[H]$ and $[G]$ have the coefficients obtained from the integrations of $\frac{\partial \ln r_{\mathrm{pq}}}{\partial \mathrm{n}}$ and $\ln r_{\mathrm{pq}}$ over the elements, respectively. In Eq. (13), on each node either ϕ is known on the free surface or ϕ_n is known on the solid surface, while at the intersection of the solid surface and the free surface, both of them are known. The number of the unknowns is the same as that of equations. This is similar to those related problems in Lu et al. [22] and Sun et al. [21, 23]

3.2. Numerical schemes for each stage

3.2.1 Water departing from the side of the body

The free surface is assumed to leave the body tangentially, and the sharp angle between the free surface and the body can lead the velocity change its direction suddenly, leading to an infinite acceleration and pressure gradient. Without loss of generality, here we may assume that at the point of the detachment, the tangential direction of body is vertical. In Eq. (5), ϕ_x and ϕ_y can then be obtained respectively from the normal and tangential velocities at the intersection. In particular, the former can be obtained from the body surface boundary condition in Eq. (6), in which $n_x = 0$ at the intersection. The potential at the point just departed from the body can be obtained from Eq. (2), which will be replaced by Eq. (4) at the later stages. After the fluid particle at the intersection point leaves from the body, a new fluid particle from the body surface will arrive at the intersection point. The velocity potential at the intersection point then becomes unknown. Together with the normal velocity of the free surface at the intersection point, there are now two unknowns at this point. As a result, there will be one more unknown than the number of equations. To resolve this, an additional equation based on interpolation is used, through the intersection point and two neighbouring points on the body surface and free surface respectively. Since the flow is assumed to leave the body

tangentially, the continuity condition of velocity in the tangential direction can be imposed at the intersection point. Thus we have [7]

$$l_{\mathrm{N}}\phi_{\mathrm{N-1}} - (l_{\mathrm{N-1}} + l_{\mathrm{N}})\phi_{\mathrm{N}} + l_{\mathrm{N-1}}\phi_{\mathrm{N+1}} = 0 \tag{14}$$

Here $\phi_{\mathrm{N-1}}$, ϕ_{N} and $\phi_{\mathrm{N+1}}$ denote the velocity potentials respectively at the points on the free surface, at the intersection and on the body surface, respectively. l_{N-1} is the distance between the former two points, and l_N is the distance between the latter two points.

3.2.2 The dual systems for stages 2(a) and 3(a)

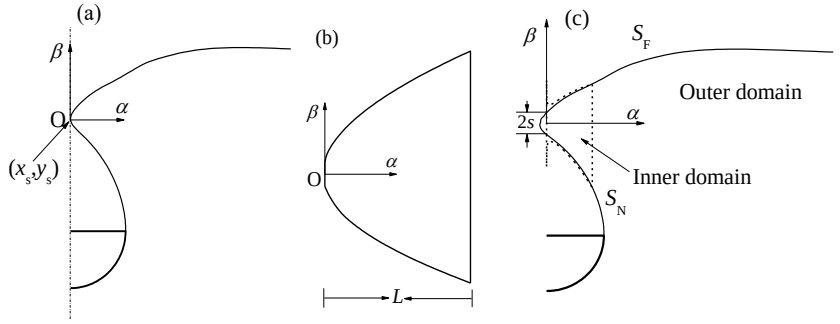

Fig. 3. The sketch for the inward free surface hitting symmetry line at stage 2(a). (a) The free surface in physical system at the moment of bubble formation (b) the initial wave profile in stretched system (c) matching between the inner and outer domains

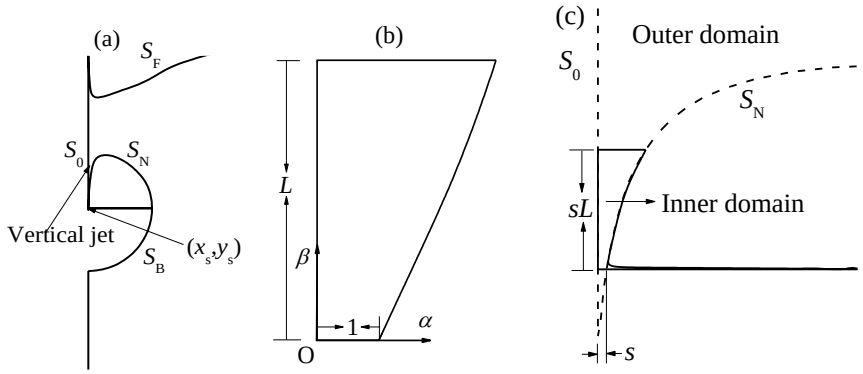

Fig. 4. The sketch for the inner vertical jet hitting the top of body at stage 3. (a) The free surface in physical system at the moment of impact (b) the initial wave profile in stretched system (c) matching between the inner and outer domains

At the moment of the free surface hitting the symmetry line in stage 2(a) or the vertical jet hitting the top of body in stage 3(a), the contact area normally starts from a single point and then increases rapidly, which leads to a major challenge in the computation as highlighted in the related work [24, 25]. To avoid numerical difficulties due to the extremely small contact area at the initial stage, the dual system method used in [20] is adopted at these two stages. In particular the stretched system $O-\alpha\beta$ [6, 23] is used within a small zone near the initial contact point $(x,y)=(x_s,y_s)$, and the physical system $O-xy$ is adopted to the whole domain as if the inward free surface had passed through an invisible wall without collision, as adopted in Sun et al. [20]. The origin of the stretched

system $O-\alpha\beta$ is set at $(x,y)=(x_s,y_s)$. At stage 2(a), the stretching ratio s is taken as the half width of intersection line between the unaffected free surface by the impact and symmetry line (Fig. 3). At stage 3(a), the stretched system moves with the body, and the stretching ratio s is taken as the length of intersection line between the vertical jet and the top of body (Fig. 4). With such a definition, we can write

$$s\alpha = x \tag{15}$$

$$s\beta = y - y_s \tag{16}$$

$$s\varphi = \phi \tag{17}$$

where $x_s = 0$ has been used in both stages 2(a) and 3(a). y_s at stage 2(a) remains fixed while it moves with the body at stage 3(a). In the stretched system, the kinematic boundary conditions can be written as

$$\frac{Ds\alpha}{Dt} = \varphi_\alpha \tag{18}$$

$$\frac{Ds\beta}{Dt} = \varphi_\beta \text{, for stage 2(a)} \tag{19}$$

$$\frac{Ds\beta}{Dt} = \varphi_\beta - W \text{, for stage 3(a)} \tag{20}$$

The dynamic boundary conditions on the inner and outer free surfaces can be respectively transformed as

$$\frac{Ds\varphi}{Dt} = \frac{1}{2}\nabla\varphi\cdot\nabla\varphi - (s\beta + y_s) - P_0\left[(\frac{V_0}{V})^\gamma - 1\right] \tag{21}$$

$$\frac{Ds\varphi}{Dt} = \frac{1}{2}\nabla\varphi\cdot\nabla\varphi - (s\beta + y_s) \tag{22}$$

At the interface of local domain with (α,β) and the result of domain with (x,y), we impose

$$\frac{\partial\varphi}{\partial n} = \frac{\partial\phi}{\partial n} \tag{23}$$

where the spatial derivatives on two hand sides of Eq. (23) are taken in the stretched and physical systems respectively. The normal derivative on the right hand side can be obtained through the interpolation from the values on the adjacent free surfaces, based on the assumption that the inward free surface would propagate forward without collision, as in Sun et al. [20].

3.2.3 Water jet in stages 2(b) and 3(b)

When the path of the liquid motion is blocked by a solid surface, its flow direction has to change suddenly to move along the surface. A thin jet is usually developed. Unless the sizes of the elements on both sides of the jet are much smaller than the jet thickness, numerical error can become significant. To ensure accuracy in such a way would lead to a large number of very small elements, which can be practically impossible. To solve this problem, the treatment for the thin layer introduced by Wu [6] is used here. Near each element, the velocity potential ϕ is assumed to vary linearly across the thin layer. Thus we have

$$\phi = A + Bx + Cy \tag{24}$$

Substituting Eq. (24) into Eqs. (6) or (7), we have

$$\begin{cases} \dfrac{\partial \phi}{\partial x} = B = 0, \ \text{stage}\,2 \\ \dfrac{\partial \phi}{\partial y} = C = W, \ \text{stage}\,3 \end{cases} \tag{25}$$

The remaining two coefficients in Eq. (24) can be obtained through the known potentials on two points on the free surface. This leads to that both ϕ and ϕ_n are known on the both sides of jet surface, and they can be moved to the right hand side of Eq. (13). In this way, the existence of the jet will not increase any computational effort.

3.2.4 Domain decomposition scheme with Riemann second sheet method for stage 3(c)

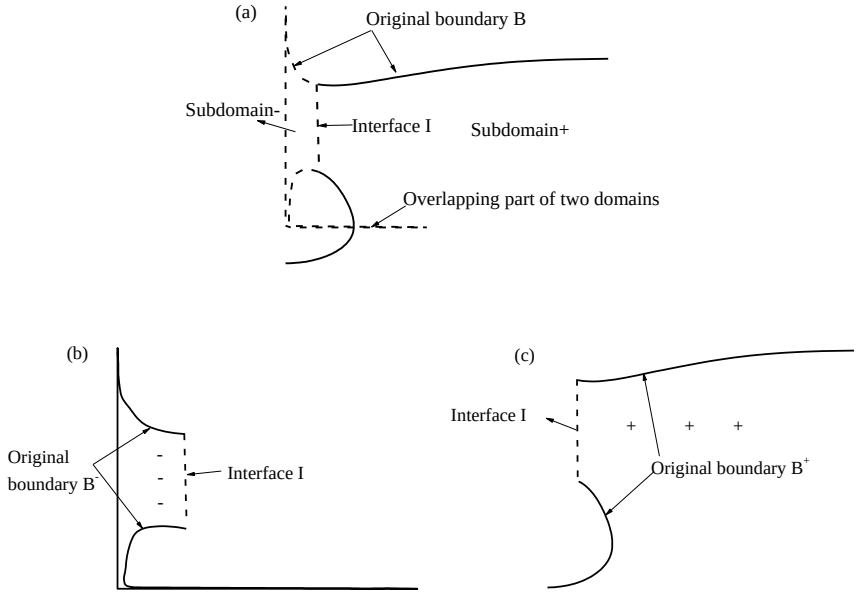

Fig. 5. The sketch of domain decomposition. (a) The horizontal jet hits the inner free surface on the top of the body, (b) the domain with the horizontal jet and (c) the rest of the domain

When the horizontal jet on the body hits the inner free surface, the entrapped air bubble may become detached from the body surface. Treatments similar to those at previous stages could be used. Alternatively, we could adopt the method of Sun et at. [21], in which the incoming jet will pass into the free surface through Riemann second sheet, as shown in Fig. 5. We notice that there is an overlapping domain in Fig. 5(a), while the boundary integral equation in Eq. (11) is for a non-overlapping domain and it cannot be used directly in such a case. To resolve this, the domain is then decomposed into two sub-domains. One of these domains, subdomain $-$, covers the area near the symmetry line, and the other, subdomain $+$, covers the rest of the fluid, and I denotes the interface between two sub-domains, as shown in Fig. 5. The boundary integral equation is used in each of the two domains separately. Continuity conditions of velocity and pressure are imposed on the interface I through applying $\phi_{\mathrm{I}^+} = \phi_{\mathrm{I}^-}$ and $\phi_{\mathrm{I}^+ n} = -\phi_{\mathrm{I}^- n}$, where I^- and I^+ mean that the interface is approached from B^- and B^+ respectively, with opposite normal directions, and the subscripts B^- and B^+ imply the values on the original boundaries of these domains. Consequently Eq. (13) can be written as [21]

$$\begin{bmatrix} H_{B^+B^+} & H_{B^+I^+} & 0 \\ H_{I^+B^+} & H_{I^+I^+} & 0 \\ 0 & H_{I^-I^-} & H_{I^-B^-} \\ 0 & H_{B^-I^-} & H_{I^-I^-} \end{bmatrix} \cdot \begin{bmatrix} \phi_{B^+} \\ \phi_{I^+} \\ \phi_{B^-} \end{bmatrix} = \begin{bmatrix} G_{B^+B^+} & G_{B^+I^+} & 0 \\ G_{I^+B^+} & G_{I^+I^+} & 0 \\ 0 & -G_{I^-I^-} & G_{I^-B^-} \\ 0 & -G_{B^-I^-} & G_{I^-I^-} \end{bmatrix} \cdot \begin{bmatrix} \phi_{B^+n} \\ \phi_{I^+n} \\ \phi_{B^-n} \end{bmatrix} \tag{26}$$

Through this equation the difficulty of the overlapping domain can be resolved. As discussed by Sun et al. [21], this method has ignored the impact force of the jet on the inner free surface by assuming that the jet moves into Riemann second sheet. Such an approximation may not truly reflect the local behaviour of the jet impact on the free surface, but it is expected not to have major effect on the global results, similar to that in Sun et al. [21].

3.3. The pressure

The pressure in the flow field can be obtained through the Bernoulli equation

$$P - P_0 = -\phi_t - \frac{1}{2}|\nabla\phi|^2 - y \tag{27}$$

The velocity potential ϕ can be solved at each time step through the numerical scheme in the previous section, from which its gradient $\nabla\phi$ can be obtained. However the temporal derivative of potential ϕ_t is still unknown explicitly. To deal with this problem, the auxiliary function method is adopted [26]. We notice that ϕ_t also satisfies the Laplace equation in the fluid domain. The normal derivative of ϕ_t on the body surface can be written as [27]

$$\frac{\partial\phi_t}{\partial n} = \dot{W}\cdot n_y - W\cdot\frac{\partial\phi_y}{\partial n} \tag{28}$$

and on $x = 0$, we have $\frac{\partial\phi_t}{\partial x} = 0$. Special attention should be paid to the acceleration in Eq. (28), which is unknown before the force is found. To decouple their nonlinear mutual dependence, we define

$$\phi_t = \chi_0 + \dot{W}\chi_1 - W\phi_y \tag{29}$$

Here $\chi_i (i = 0,1)$ satisfy the Laplace equation. The body surface boundary conditions for the auxiliary functions can respectively be written as

$$\frac{\partial\chi_0}{\partial n} = 0 \tag{30}$$

$$\frac{\partial\chi_1}{\partial n} = n_y \tag{31}$$

On the symmetry line $x = 0$,

$$\frac{\partial\chi_0}{\partial n} = 0 \tag{32}$$

$$\frac{\partial\chi_1}{\partial n} = 0 \tag{33}$$

Considering the dynamic boundary conditions for ϕ_t on the free surface, we have

$$\chi_0 = -\frac{1}{2}|\nabla\phi|^2 - y - P_0\left[\left(\frac{V_0}{V}\right)^{\gamma} - 1\right] + W\phi_y, \text{ on } S_F \tag{34}$$

$$\chi_0 = -\frac{1}{2}|\nabla\phi|^2 - y + W\phi_y, \text{ on } S_N \tag{35}$$

and

$$\chi_1 = 0, \text{ on } S_F \text{ and } S_N \tag{36}$$

At the bottom of the fluid, the boundary conditions for these two functions become

$$\frac{\partial\chi_0}{\partial n} = -W\frac{\partial^2\phi}{\partial y^2} \tag{37}$$

$$\frac{\partial\chi_1}{\partial n} = 0 \tag{38}$$

At the far field, the boundary conditions can be written as

$$\frac{\partial\chi_i}{\partial n} = 0, (i = 1, 2) \tag{39}$$

When the air cavity has been formed, the pressure along the top of body will change with the compression and expansion of air bubble, based on Eq. (3). When the vertical jet hits the top of body, the dual system method can be used for the potential. The pressure on the wetted part of the body top is calculated in the stretched system [20], while that on the part in touch with air is obtained through Eq. (3).

3.4. The motion of body

Based on Newton's law, the equation for motion of the body can be written as

$$m\dot{W} = f - m \tag{40}$$

where m is the mass of body, and f is the fluid force, which can be obtained through the integration of pressure $P - P_0$ along the body surface including its top. Thus we have

$$f = -\int_{S_W}(\phi_t + \frac{1}{2}|\nabla\phi|^2 + y)n_y dS + \int_{S_A}(P - P_0)n_y dS \tag{41}$$

in which S_W and S_A correspond to the body surface contacting water and air respectively. Substituting Eqs. (29) and (41) into Eq. (40), it gives [6]

$$(m + c)\dot{W} = q - m \tag{42}$$

where c is the added mass defined as

$$c = \int_{S_W}\chi_1 n_y dS \tag{43}$$

and q can be obtained through

$$q = -\int_{S_W}(\chi_0 - W\phi_y + \frac{1}{2}|\nabla\phi|^2 + y)\cdot n_y dS + \int_{S_A}(P - P_0)n_y dS \tag{44}$$

4. Numerical results and discussions

4.1. Convergence study

In order to verify the reliability and accuracy of the methodology and numerical procedure in the paper, the convergence study is made through a semi-floating circle moving into deep water, with its radius being taken as the length scale for nondimensionalisation. Simulations are first undertaken

with respect to the half width L_C and depth L_D of the rectangular computational domain. It is found that when they are set as $L_C = 20$ and $L_D = 30$ respectively, the results no longer change graphically when they further increase. In the mesh convergence study, the elements of equal size l_m are distributed along the body surface, symmetry line and inner free surface, while on the outer free surface, the size of element increases gradually at a fixed ratio δ, with an upper limit of 0.5 or half of the radius of the cylinder. Special attention should be paid to the local stretched systems in stages 2(a) and 3(a), in which the truncated boundary L is set as 4 in stage 2(a) and 100 in stage 3(a) respectively. The symmetry line and the top of body are discretized with elements of equal length l_m. Away from the symmetry line and the body top, the size of element increases gradually at the ratio δ, and the largest element size is not allowed to be bigger than 0.3.

We set the element length l_m as 0.02, 0.03 and 0.04 respectively, and element size increase ratio δ as 1.02. The time histories of vertical velocity and the formed air bubble volume are provided for the body moving into water in free fall motion after being given an initial velocity W_0. Results are shown in Fig. 6, with the initial velocity W_0 and half mass m of the body being set as -1 and 3.0 respectively, and the initial buoyancy of half of the body is equal to $\pi/4$. The time step is set as $l_m / (\mu V_{max})$, where V_{max} is the maximum of the velocity magnitude on both inner and outer free surfaces at each time step and μ is a coefficient and is taken as 10. The simulation covers all three stages, the results from three sets of meshes are in good agreement, and the average relative errors are only 0.25% in Fig. 6(a) and 0.12% in Fig. 6(b) respectively. This confirms mesh convergence. To test the time step convergence, Fig. 7 provides the comparison of results from $\mu = 5$, $\mu = 10$ and $\mu = 20$ respectively with $l_m = 0.03$. It can be seen that the three curves coincide well. The average relative errors are only 0.4% in Fig. 7(a) and 0.15% in Fig. 7(b) respectively. Thus in the following simulations, unless it is specified, the element length l_m is set as 0.03, and the coefficient μ as 10.

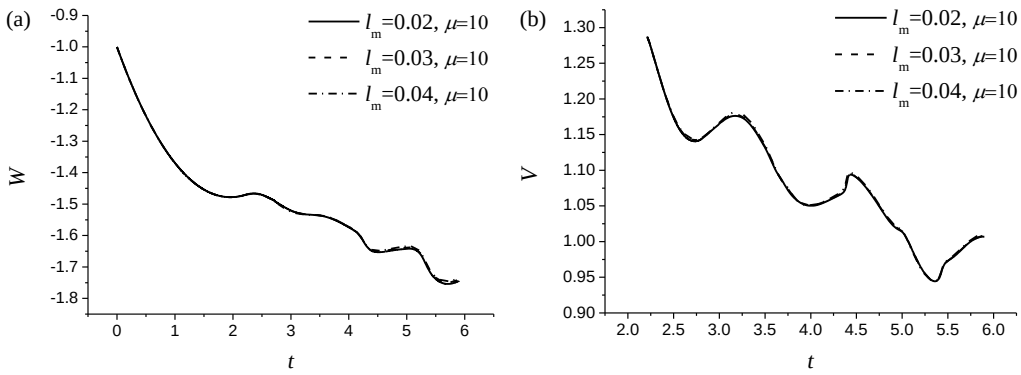

Fig. 6. Mesh convergence study through a semi-circular body falling into water freely with $W_0 = -1$. (a) Vertical velocity, (b) air bubble volume

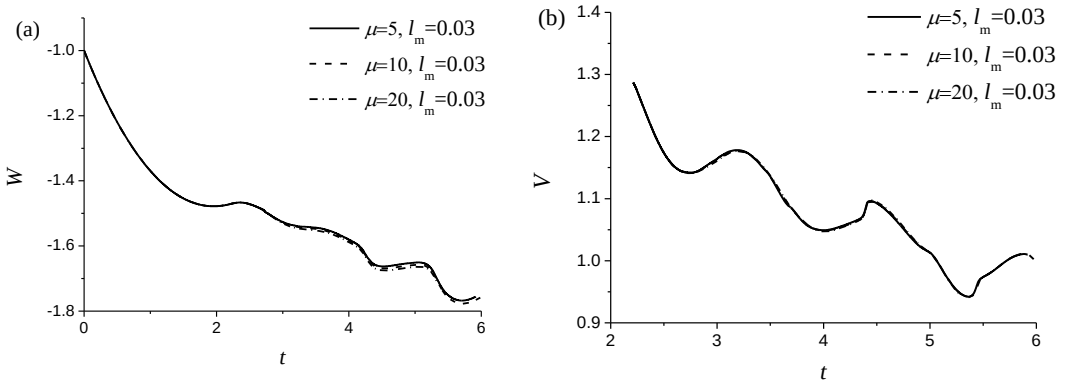

Fig. 7. Time step convergence study through a semi-circular body falling into water freely with $W_0 = -1$. (a) Vertical velocity, (b) air bubble volume

4.2. The influence of the body motion

The shape of free surface and the location of bubble closure very much depend on the motion of body. To study such an effect, the body is forced to move into water with the prescribed constant velocity or constant non-zero acceleration. As the body moves into water, the free surface first moves up in the form of splash, and the inner free surface moves inwards due to the push of water outside. After that, the gravity takes its effect, and the tip of inward free surface goes down. The root, or the detachment zone, of the free surface has an upward tendency as the body moves down further. Eventually, the inward free surface would touch the symmetry line, and an air bubble would be formed behind the body. Fig. 8 gives the free surface profile for the body arriving at the same location y_0 with different velocities W, which are -3, -5 and -7 respectively. It is evident that after nondimensionalisation, the magnitude of W is the Froude number. From the Fig. 8(a), it can be seen that the free surface for $W = -3$ tends to move inwards, while curves for $W = -5$ and -7 are close to each other. This is because at a higher W, the gravity effect is smaller for the body arriving at the same location. Mathematically, this can be clearly seen if ϕ is replaced by $W\varphi$ and t is replaced by y_0 / W in Eqs. (1~6). At large $|W| \to \infty$, the result will depend only on y_0, or at the same y_0, the result will be same. For any finite W, when y_0 is not large and $|W|$ is very large, the gravity can be neglected. The gravity effect will increase as the body moves further down. The difference between the free surface profiles at different velocities therefore becomes increasingly significant. In Fig. 8(c), for the case of $W = -3$, the bubble is already well developed and the inner jet along the symmetry line has hit the body surface, and the generated horizontal jet has moved into the Riemann second sheet. For $W = -5$ the open cavity surface has significantly moved towards the symmetry line. For $W = -7$ on the other hand, no significant inward motion of the cavity surface has occurred.

Fig.9 provides the pressure distribution along the body surface. The horizontal axis l_x is the arc

length along the body surface, starting from the middle point of its horizontal top. Similar to the free surface distribution, at a given y_0 the gravity effect is more important at smaller W and the result will not significantly be affected by W when it is sufficiently large. This is clearly reflected in the figure. In Figs. 9(a) and 9(b), the bubble has not formed. The pressure on the top of the body remains to be atmospheric. Bubble has been well developed in Fig. 9(c) for the case of $W=-3$. A particular attention should be paid to the region of $l_x < 0.1$, where a large peak can be observed. This is caused by the collision of the inner jet on the symmetry line with the top of body. Outside this region, the body top is in contact with the air bubble and the pressure is constant. Because of the compression of the air bubble from its initial volume, the pressure P is larger than P_0. The pressure remains constant until $l_x = 1$. We notice that just after the detached point $l_x > 1$, the pressure becomes negative, or P is lower than the atmospheric pressure P_0. Based on Eq. (27), the pressure contains unsteady part $-\phi_t$, velocity square part $-\frac{1}{2}|\nabla\phi|^2$ and hydrostatic part $-y$. Because the second term is always negative, it is not possible to always rule out the negative pressure. In reality, the air could be sucked into that part and the flow detachment point may move downwards as a result. Here, we shall fix the detachment point to investigate the subsequent bubble formation and its effect.

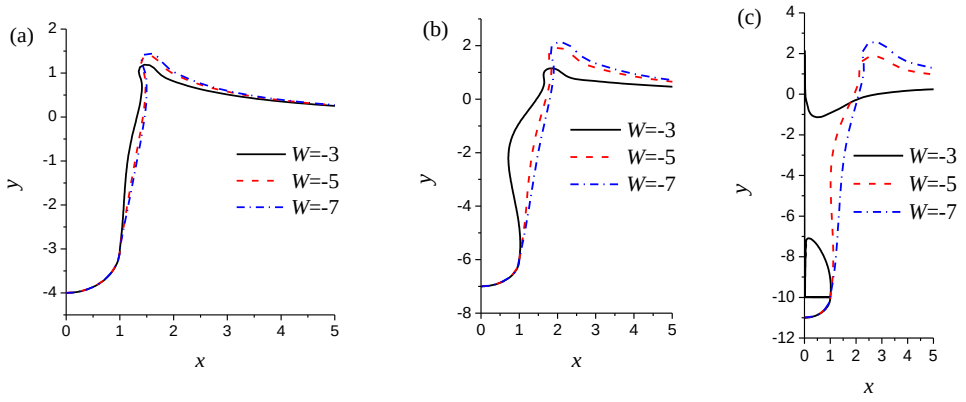

Fig. 8. The free surface profile for the body moving into water at different constant velocities. (a) $y_0 = -3$ (b) $y_0 = -6$ (c) $y_0 = -10$

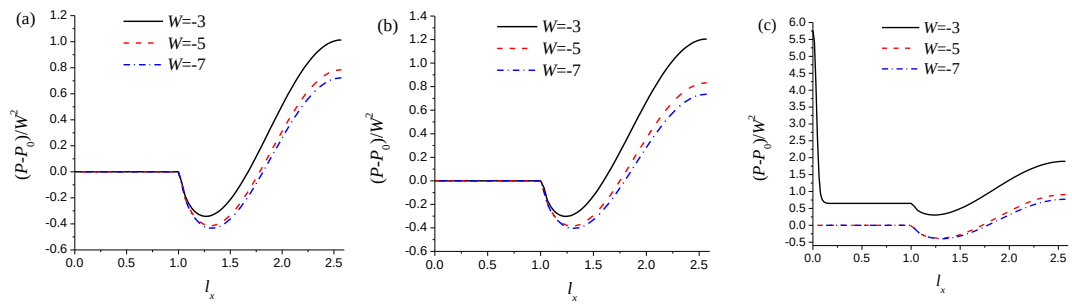

Fig. 9. Pressure distribution along the body surface, arc length l_x is measured from the middle of the horizontal top of the body until its lowest point. (a) $y_0 = -3$ (b) $y_0 = -6$ (c) $y_0 = -10$

The case considered above corresponds to $\dot{W} = 0$. We now consider the case of a body starting with an initial falling velocity W_0 and a constant acceleration $\dot{W}$. When the body reaches y_0, we have $2y_0 a + W_0^2 = W^2$, in which a denotes the acceleration $\dot{W}$. Substituting this equation into Eqs. (2) and (4) after replacing ϕ with $W\varphi$ and $\partial/\partial t$ with $W\,\partial/\partial y_0$, we can find that there is an extra term $\frac{a\varphi}{W^2}$. For a given W_0, the solution depends on a and y_0 explicitly. If we ignore the last term in Eq. (2) due to gravity, we can find that when $W_0 = 0$, the solution will depend on y_0, but not a explicitly. This is similar to what has been observed by Sun et al. [21] on the slamming of a rotating flap. For the general cases with $W_0 \neq 0$, when y_0 is small or at the initial stage, the term $a\varphi$ is small as $\varphi = 0$ at $t = 0$. Thus all results at different a will be close to each other. Fig. 10 gives the free surface profiles for the body with $W_0 = -3$ at different accelerations. At $y_0 = -3$, the free surface profiles with different accelerations are very close and the air bubble has not formed yet, even though the velocity of body is different, as seen in Fig. 10(a). When y_0 is not small, the acceleration will start to take effect, while the larger a will make the gravity effect less prominent. This is why at $y_0 = -6$ the inward tendency is most prominent for the case $a = 0$, as shown in Fig. 10(b). The gravity effect will further increase as the body moves down further. Thus the difference of free surface profiles will become more prominent, as can be seen in Fig. 10(c). Specifically, the air bubble for $a = -0.8$ with smallest gravity effect is in the middle of formation, while the free surface has hit the symmetric line for $a = -0.4$, and for $a = 0$ the air bubble has already formed and the horizontal jet has already moved into Riemann second sheet. If we make a comparison between the curves for $a = -0.8$ in Fig. 10(a) and $a = -0.4$ in Fig. 10(b), it can be found that the inward tendency for the latter is more prominent, which further shows that the larger acceleration can make the gravity effect become smaller.

Fig. 11 gives the pressure distribution along the body surface, similar to Fig. 9. Before the formation of the air bubble, see Figs. 11(a) and (b), the pressure $P - P_0$ on the top of the body ($l_x < 1$) in contact with air is zero. Along the side of the body to its bottom ($l_x \geq 1$) in contact with water, the fluid pressure first decreases, and then increases to a peak at the bottom. For larger $|a|$,

the pressure experiences a larger drop and reaches a higher peak. At $y_0 = -10$, air bubble has formed for the cases of $a = 0$ and -0.4, as can be seen in Fig. 10(c). In the former, the inner jet has hit the top of the body, leading to a peak pressure at $l_x = 0$. In the latter, the inner jet has not reached the top of the body and the pressure near $l_x = 0$ is still the bubble pressure which is slightly higher than P_0.

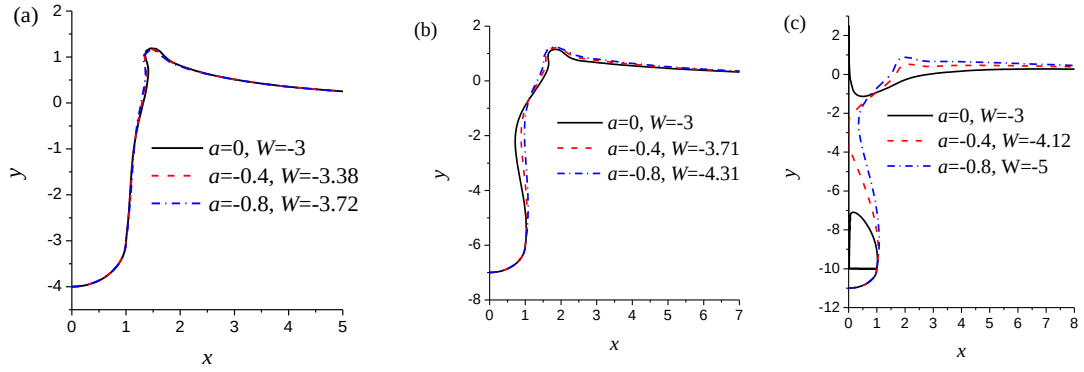

Fig. 10. The free surface for the body moving into water with $W_0 = -3$ at different constant accelerations. (a) $y_0 = -3$ (b) $y_0 = -6$ (c) $y_0 = -10$

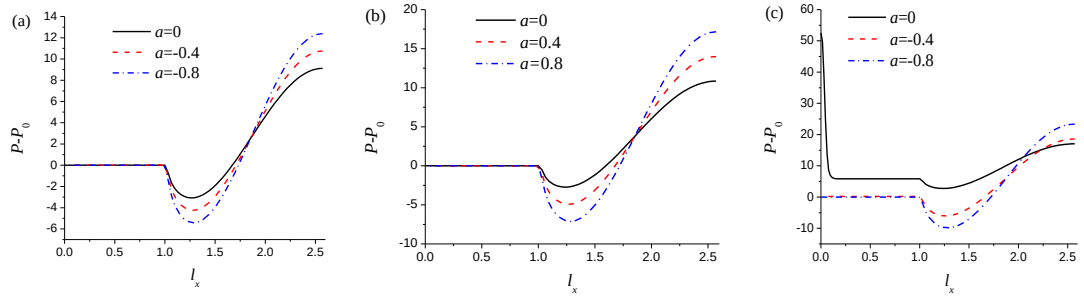

Fig. 11. Pressure distribution along the body surface, arc length l_x is measured from the middle of the horizontal top of the body until its lowest point. (a) $y_0 = -3$ (b) $y_0 = -6$ (c) $y_0 = -10$

4.3. The effect of initial velocity in free motion

We then consider the case of a semi-circular body falling into water freely at different initial velocities W_0. The half of the body mass m is set as 3, and half of the initial buoyancy is $\pi / 4$. The acceleration is now part of the solution and will depend on W_0 for a given m. Thus the result at a given y_0 will be a function of W_0. Fig. 12 provides the variations of the velocity of body before bubble closure with $|y_0|$, and those of the velocity, as well as the volume and pressure of air

bubble with $|y_0 - y_{0s}|$, after closure. The subscript s denotes the moment when the air bubble has formed. At the initial stage, the acceleration of the body depends on the difference between body weight and the fluid force. The former is fixed while the latter varies with W_0. For $W_0 = 0$, the acceleration can be obtained easily from Eq. (42) as all the terms in Eq. (44) are zero apart from the term of y, which is the static upwards buoyancy and is smaller than the body weight. As a result the body acceleration will be smaller than that due to gravity. For a small non-zero W_0, the upward forward force will increase and the initial acceleration will further decrease. As the magnitude of W_0 increases, the upward forward force will become larger than the weight, and the acceleration will become deceleration. In Fig. 12(a), the latter cases could be seen by the initial slopes of W. As the deceleration increases with the initial velocity, the difference between the velocities becomes smaller as y_0 increases. As the body moves down, an air bubble is formed behind the body. Its volume and pressure oscillate with y_0. We can expect that after a sufficiently long period of time, W may become a constant when the fluid force is in balance with the body weight, especially if the air bubble has become detached from the body and moved away. W may also continue to be an oscillatory function of y_0, especially if the bubble remains to be attached or close to the body. However these are physical phenomena which are beyond the scope of the present work and are not part of the focus of this study.

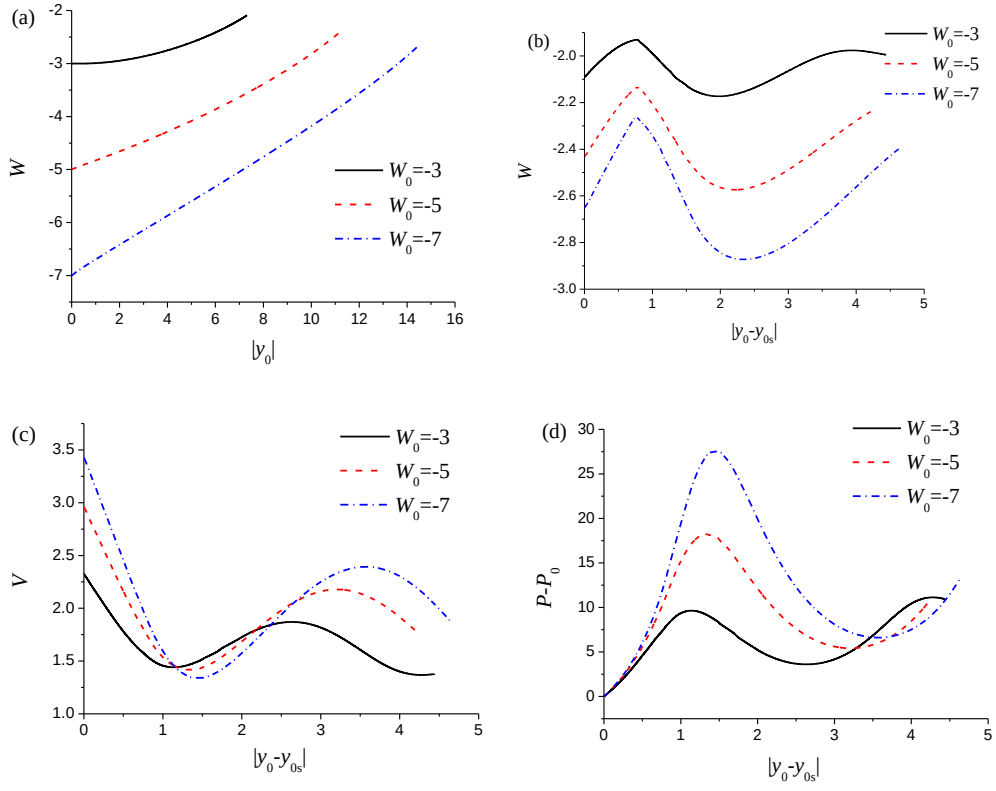

Fig. 12. Free fall of a semi-circular body with different initial velocities. (a) & (b) The velocity of the body before and after bubble closure, respectively, (c) & (d) volume and pressure of the air bubble, respectively

The free surface profiles at different y_0 are provided in Fig. 13. When the body arrives at $y_0 = -3$, the magnitudes of the velocity for these cases have decreased to 2.87, 4.48 and 6.14 respectively, as shown in Fig. 13(a). However, all the free surface profiles are very similar to those from Fig. 8(a). The principal reason for this is that the decrease of velocity is relatively small, or W is still relatively close to W_0. When the body has arrived at $y_0 = -6$ in Fig. 13(b), a more obvious difference can be found between the free surfaces in Figs. 8(b) and 13(b). Specifically, the inward tendency becomes more prominent in Fig. 13(b) due to the decrease of velocity. Such a tendency continues as the body arrives at $y_0 = -10$ in Fig. 13(c). The deceleration begins to take more evident effect, the velocity has decreased significantly. Thus in Fig. 13(c), the inward tendency for $W_0 = -5$ is noticeably more prominent than its corresponding free surface shape in Fig. 8(c).

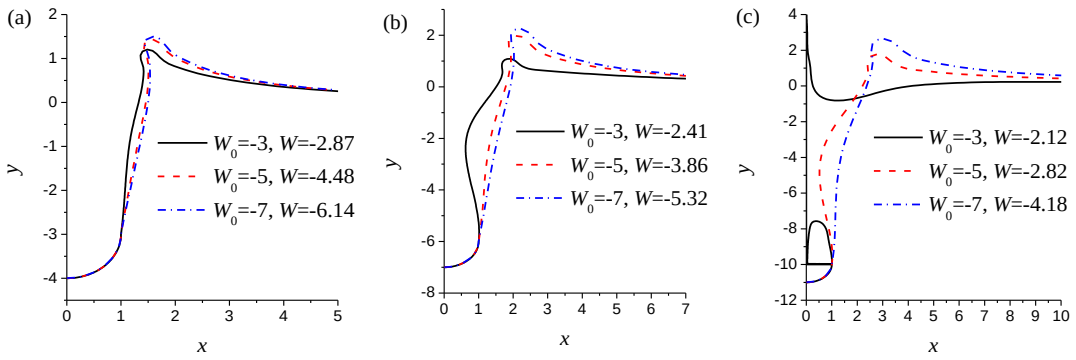

Fig. 13. The free surface for the body moving into water freely at different initial velocities. (a) $y_0 = -3$ (b) $y_0 = -6$ (c) $y_0 = -10$

4.4. The effect of body mass in free motion

We then consider the case of a semi-circular body falling into water freely with different half body masses, which are set as $m = 3$, 6 and 9 respectively, and half of the initial buoyancy is $\pi / 4$. The initial velocity of the body is taken as W_0=-3, and the acceleration and subsequent velocity will be part of the solution. Fig. 14 provides the variations of the velocity of the body before bubble closure with $|y_0|$ and those for the velocity, as well as the volume and pressure of air bubble after closure with $|y_0\text{-}y_{0s}|$. At $|y_0| = 0$, the fluid force does not depend on m and is obviously upward when $W_0 < 0$. For a body with a smaller mass, it will start with the deceleration because its mass will be smaller than the fluid force, which can be seen from the initial slope of the W

curve of $m=3$ in Fig. 14(a). On the other hand, as the body weight increases, it will accelerate as can also be seen in the figure. Thus the difference of velocities will increase continually for a while. After bubble formation, as the air bubble volume first decreases with the inner free surface moving down, and its internal pressure therefore increases, as seen in Fig. 14(d). The increased air bubble pressure will slow the inner free surface moving downwards and speed up the falling body, and therefore its volume will bounce back or increase. The pressure in the bubble will then decrease, but it is still above the atmospheric one, which means the bubble is still in compression. In Fig. 14(b), it can be seen that the motion of the body is noticeably affected by the oscillation of the air bubble pressure.

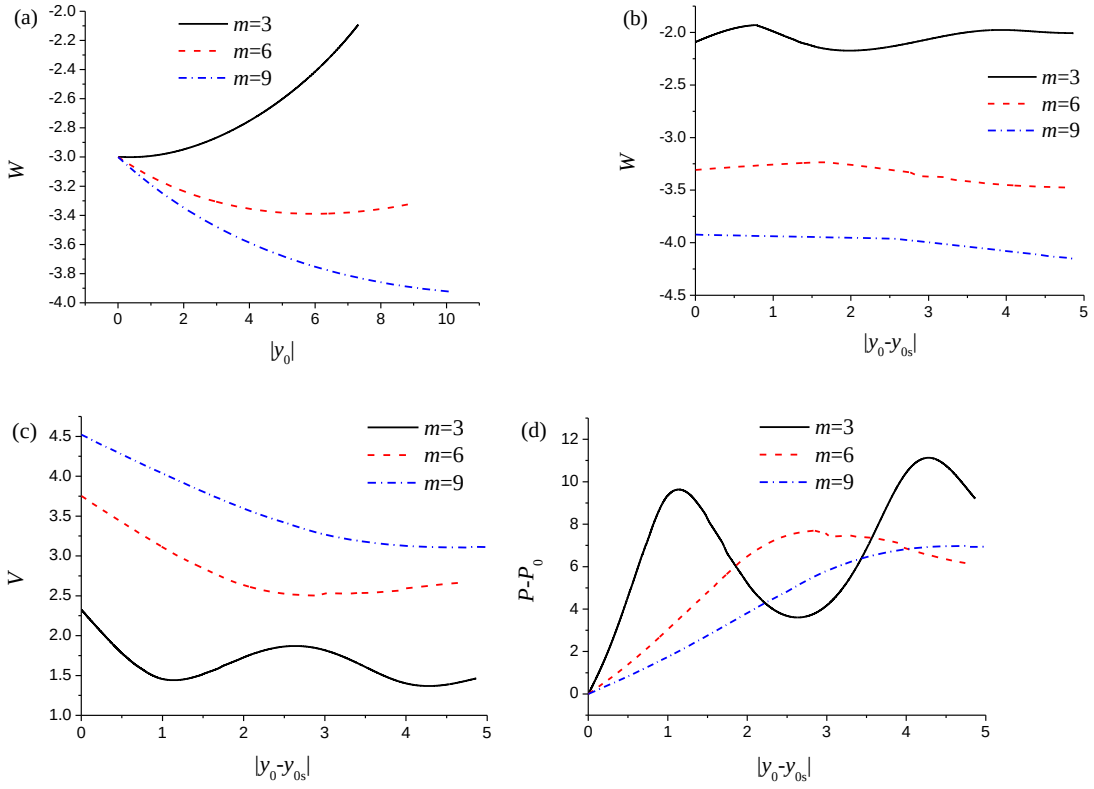

Fig. 14. Free fall of semi-circular bodies with different half body masses. (a) & (b) The velocity of the body before and after bubble closure, respectively, (c) & (d) volume and pressure of the air bubble, respectively

The free surface profiles at different y_0 are provided in Fig. 15. When the body arrives at $y_0=-3$, the magnitude of velocity for 3.0 has decreased to 2.87, while those for $m=6$ and 9 have increased to 3.31 and 3.48 respectively. The free surface profiles are very close, as shown in Fig. 15(a), as the difference between the velocities are still not big enough and the falling time is not sufficiently long. As y_0 reaches -6 in Fig. 15(b), the velocity magnitude for $m=3$ has decreased to 2.41, which is much smaller than the other two cases. This leads to a more noticeable gravity effect, which makes the inner free surface move inwards. As the body moves down further to $y_0=-10$, the difference between velocities continues to increase. The velocity magnitude for

$m=9$ is about the twice as that for $m=3$. The difference in free surface profiles therefore becomes evident. In Fig. 15(c), the horizontal jet on the top of the body for $m=3$ has already travelled into Riemann second sheet, and the vertical jet has formed for $m=6$ and the inner free surface for $m=9$ has just touched the symmetric line.

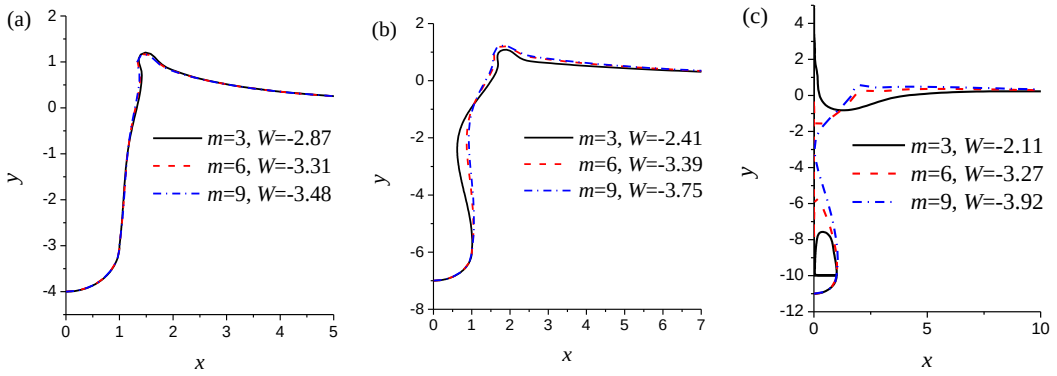

Fig. 15. The free surface for the body moving into water freely at different half body masses. (a) $y_0=-3$ (b) $y_0=-6$ (c) $y_0=-10$

5. Conclusions

The problem of a floating body sinking into water in either forced motion or in free fall with entrapped air bubble effect has been modelled using velocity potential theory with fully nonlinear boundary conditions on the free surface. It is solved through the boundary element method. The problem is divided into several stages, and specific methods, through dual coordinate systems, domain decomposition with Riemann second sheet and auxiliary functions, have been adopted to resolve the numerical difficulty at each stage. Extensive simulations have been undertaken for the dynamic features of the air bubble formed behind the body at different motion modes, from which the following conclusions can be drawn.

(1) The gravity effect is unimportant when the distance that the body has travelled is small. It becomes increasingly important for deformation of the open cavity, the formation of the air bubble and pressure distribution as the body moves downwards.

(2) When the air bubble is formed, its internal pressure is initially equal to the atmospheric one. Subsequently, the air pressure remains to be larger than the atmospheric one, or the bubble is always in compression in the whole period of simulation, although it may oscillate when the body moves down. The bubble therefore generally contributes to a downward force on the body.

(3) When the body enters water at constant velocity or constant acceleration, the gravity effect will become less prominent and the formation of the air bubble will be delayed, when their magnitudes increase. When they become very large, the result will mainly depend on the distance that the body has travelled.

(4) In free fall motion, for the body with a given mass, a larger initial velocity leads to a larger upward forward force, which will create a larger deceleration. As a result the body will slow down more quickly. In such a case, initially different entry velocities will become closer as the body moves down. On the other hand, if the initial entry velocity is the same, different body masses will lead to different velocities subsequently.

Acknowledgement

This work is supported by Lloyd's Register Foundation through the joint centre involving

University College London, Shanghai Jiaotong University and Harbin Engineering University, to which the authors are most grateful. Lloyd's Register Foundation helps to protect life and property by supporting engineering-related education, public engagement, and the application of research.

This work is also supported by the National Natural Science Foundation of China (Grant No. 51879123, 51809123) and the Key University Science Research Project of Jiangsu (18KJA130001).

References

[1] D. Gilbarg, R.A. Anderson, Influence of atmospheric pressure on the phenomena accompanying the entry of spheres into water, J. Appl. Phys. 19 (1948) 126-139.

[2] E.G. Richardson, The sounds of impact of a solid on a liquid surface, Proc. Phys. Soc. B 68 (1955) 541-547.

[3] C. Duez, C. Ybert, C. Clanet, L. Bocquet, Making a splash with water repellency, Nature Phys. 3 (2007) 180-183.

[4] Z.N. Dobrovol'skaya, On some problems of similarity flow of fluid with a free surface, J. Fluid Mech. 36 (1969) 805–829.

[5] R. Zhao, O. Faltinsen, Water entry of two-dimensional bodies, J. Fluid Mech. 246 (1993) 593-612.

[6] G.X. Wu, H. Sun, Y.S. He, Numerical simulation and experimental study of water entry of a wedge in free fall motion, J. Fluids Struct. 19 (2004) 277-289.

[7] C.M. Bao, G.X. Wu, G.D. Xu, Simulation of water entry of a two-dimension finite wedge with flow detachment, J. Fluids Struct. 65 (2016) 44-59.

[8] C.M. Bao, G.X. Wu, G. Xu, Water entry of a finite width wedge near a floating body, Appl. Ocean Res. 84 (2019) 12-31.

[9] R. Zhao, O. Faltinsen, J. Aarsnes, Water entry of arbitrary two-dimensional sections with and without flow separation, Twenty-First Symposium on Naval Hydrodynamics, 1997.

[10] J. Wang, O.M. Faltinsen, Numerical investigation of air cavity formation during the high-speed vertical water entry of wedges, J. Offshore Mech. Arct. Eng. 135 (2013) 011101.

[11] A.A. Korobkin, G.X. Wu, Impact on a floating circular cylinder, Proc. R. Soc. Lond. 456 (2000) 2489-2514.

[12] M. Do-Quang, G. Amberg, The splash of a solid sphere impacting on a liquid surface: Numerical simulation of the influence of wetting, Phys. Fluids, 21 (2009) 022102.

[13] A. Iranmanesh, M. Passandideh-Fard, A three-dimensional numerical approach on water entry of a horizontal circular cylinder using the volume of fluid technique, Ocean Eng. 130 (2017) 557-566.

[14] T. Grumstrup, J.B. Keller, A. Belmonte, Cavity ripples observed during the impact of solid objects into liquids, Phys. Rev. Lett. 99 (2007) 114502.

[15] M. Minnaert, On musical air-bubbles and the sound of running water, Phil. Mag. 16 (1933) 235-248.

[16] J.M. Aristoff, J.W.M. Bush, Water entry of small hydrophobic spheres, J. Fluid Mech. 619 (2009) 45-78.

[17] J. Wang, C. Lugni, O.M. Faltinsen, Experimental and numerical investigation of freefall wedges entering the water surface, Appl. Ocean Res. 51 (2015) 181-203.

[18] M. Hattori, A. Arami, T. Yui, Wave impact pressure on vertical walls under breaking waves of various types, Coast. Eng. 22 (1994) 79-114.

[19] T.G. Shepard, S. Kane, S. Wielgos, A. Eshmawy, Trajectory model for vertical sphere water

entry in presence of deep-seal cavity, Appl. Ocean Res. 82 (2019) 478-488.
[20] S.Y. Sun, G.X. Wu, G. Xu, Breaking wave impact on a floating body with air bubble effect, J. Fluids Struct. 82 (2018) 16-34.
[21] S.Y. Sun, S.L. Sun, H.L. Ren, G.X. Wu, Splash jet and slamming generated by a rotating flap, Phys. Fluids, 27 (2015) 092107.
[22] C.H. Lu, Y.S. He, G.X. Wu, Coupled analysis of nonlinear interaction between fluid and structure during impact, J. Fluids Struct. 14 (2000) 127-146.
[23] S.Y. Sun, S.L. Sun, G.X Wu, Oblique water entry of a wedge into waves with gravity effect, J. Fluids Struct. 52 (2015), 49-64.
[24] K. Tanizawa, D.K.P. Yue, Numerical computation of plunging wave impact loads on a vertical wall. Part 2. The air pocket, Proceedings of 7th International Workshop on Water Waves and Floating Bodies, Val de Reuil, France, 1992.
[25] S. Zhang, D.K.P. Yue, K. Tanizawa, Simulation of plunging wave impact on a vertical wall, J. Fluid Mech. 327 (1996) 221–254.
[26] G.X. Wu, R. Eatock Taylor, The coupled finite element and boundary element analysis of nonlinear interactions between waves and bodies, Ocean Eng. 30 (2003) 387-400.
[27] G.X. Wu, Hydrodynamic force on a rigid body during impact with liquid, J. Fluids Struct. 12 (1998) 549 – 559.